1476. An analytical model for dynamic simulation of the composite rotor with internal damping

Yongsheng Ren[1], Xingqi Zhang[2], Yanghang Liu[3], Xiulong Chen[4]
College of Mechanical and Electronic Engineering, Shandong University of Science and Technology, Qindao, 266590, China
[1]Corresponding author
E-mail: [1]*renys@sdust.edu.cn*, [2]*zhifengqx@163.com*, [3]*1020003247@qq.com*, [4]*cxldy99@163.com*
(Received 3 September 2014; received in revised form 4 November 2014; accepted 19 November 2014)

Abstract. A theoretical model for the dynamics of composite rotor is presented. The composite shaft that includes rigid disks and is supported on rigid bearings is considered as a thin-walled Euler-Bernoulli beam. Internal damping of the composite shaft is taken into account. The equations of motion are derived using the thin-walled composite beam theory based on variational asymptotic method and Hamilton's principle. The internal damping of shaft is introduced by adopting the multi-scale damping analysis method. Galerkin's method is used to discretize and solve the governing equations. To demonstrate the validity of the present model, the convergence of the method is examined and the results are compared with those available in the literature. Numerical study shows the effect of design parameters on the natural frequencies, critical rotating speeds and instability thresholds of composite shaft. In addition, the free vibration responses due to the initial perturbations and the forced responses to unbalance for composite shaft are also presented.

Keywords: composite shaft, internal damping, vibration and stability.

1. Introduction

The rotating composite shaft is the primary component for helicopter power transmission and automotive drive system. This can be attributed to the improved properties of composites, such as high strength and stiffness as well as light-weight, compared to metals. On the other hand, composites have excellent damping characteristics, which make them play an important role on damping vibration of laminated plate and shell-like non-rotating structures [1]. Unfortunately, as the rotating speed is in the supercritical range, such damping may cause whirl instabilities of composite shaft. In the field of rotor dynamics, the damping in the composite shaft is called internal damping, which is also called rotating damping. Bucciarelli [2] demonstrated that increasing internal damping may reduce the instability threshold, whereas, the addition of external damping can improve rotor stability. Internal damping characteristics is very important for dynamical stability of composite shaft. Moreover, the destabilizing effect of internal damping can be easily influenced by the arrangement of the different composite layers: fiber orientation angles and number of layers. With the increasing demand for high speed composite rotors, the study of composite shaft based on accurate prediction of internal damping is becoming fundamental as it will provide more reasonable and safe rotor design.

The study of rotating shaft with internal damping was first presented by Kimball [3]. His's results exhibited that internal damping causes shaft whirling above the first critical speed. Gunter [4] illustrated how above the first critical speed, internal viscous damping leads to instability in the rotating shaft. Vance and Lee [5] studied the stability of high speed rotors with internal viscous damping. The model they used included a single unbalance disk connected with a flexible shaft. The stability was predicted using mathematical methods and verified by numerical solutions of the equation of motion. Melanson and Zu [6] performed vibration analysis of an internally damped rotating shaft, modeled using Timoshenko shaft theory. Explicit analytical expressions for the complex frequencies and mode shapes were presented and the stability threshold was also determined. Montagnier and Hochard [7] studied dynamic instability of supercritical driveshaft with internal damping based on Euler-Bernoulli shaft model. The model taken into account the

effect of translational and rotatory inertia. Simon and Flowers [8] presented an investigation of using adaptive control method to suppress instability and synchronous disturbance of a flexible shaft with internal viscous damping. However, all these foregoing literatures deal with only rotating metal shaft.

In recent years, dynamic analysis of the composite shaft with internal damping has also received some attention [9-11]. Singh and Gupta [9] presented the rotordynamic formulations which are applicable to the analysis of the composite shaft with internal damping, obtained by using a layerwise beam theory. Kim et al. [10] conducted the forced vibration analysis of a rotating tapered composite shaft. The stability of a rotating shaft driven through a universal joint has been investigated by Mazzei and Scott [11]. In the above studies, an equivalent viscous damping coefficient was introduced to account for the effect of composite internal damping, but no internal damping analysis has been proposed. To our best knowledge, very few models which incorporate damping estimations are available for predicting the dynamic behavior of composite shaft. Sino et al. [12] presented a dynamic analysis of composite rotating shaft. Internal damping was introduced by the complex constitutive relation of a viscoelastic composite.

The internal damping of composite shaft mainly comes from the dissipation of energy in the materials. Saravanos et al. [13] presented a hollow tubular beam finite element model to predict the damping properties of anisotropic thin-walled closed-section structures. However, this model is only applicable to non-rotating composite beams or blades.

An analytical model of rotating composite thin-walled shaft including internal damping is proposed. This model is based on the composite thin-walled beam theory, referred to as variational asymptotically method (VAM) by Berdichevsky et al. [14]. The internal damping of shaft is introduced via the multi-scale damping mechanics [15]. The flexible composite shaft is assumed supporting on on rigid bearings and containing of the rigid disks mounted on it. The equations of motion of the composite shaft are derived by Hamilton's principle. Galerkin's method is used then to discretize and solve the governing equations. The natural frequencies, critical rotating speeds, instability thresholds are obtained through numerical simulations. The effect of the ply angle is then assessed. The validity of the model is proved by comparing the results with those in literatures and convergence examination. Finally, the transient free vibration responses due to the initial perturbations and the steady state forced responses to unbalance are also obtained by using the time-integration method and the mode superposition method, respectively.

2. Composite shaft

The slender thin-walled composite shaft subjected to a rotation along its longitudinal x-axis at a constant rotating speed Ω is shown in Fig. 1. The length, wall thickness and radius of the shaft are denoted by L, h and r, respectively. To describe the motion of the shaft the following coordinate systems are used: (I) (X, Y, Z) is inertial reference system whose origin O is located in the geometric center, (II) (x, y, z) is rotating reference system with the common origin O. (I, J, K) and (i, j, k) denote the unit vectors of the reference system (X, Y, Z) and (x, y, z), respectively. In addition, a local coordinate system (ς, s, x) is used, where ς and s are measured along the direction normal and tangent to the middle surface, respectively.

The variation of the strain energy of the cross-section can be expressed as:

$$\delta U_s = \int_A \delta \boldsymbol{\varepsilon}_{x,y}^T \overline{\mathbf{Q}}_{ij} \boldsymbol{\varepsilon}_{x,y} ds d\varsigma, \tag{1}$$

where $\boldsymbol{\varepsilon}_{x,y}^T = \{\gamma_{11} \quad \gamma_{12} \quad 2\gamma_{12}\}$, $\gamma_{\alpha\beta}$ $(\alpha, \beta = 1, 2)$ are the in-plane tensorial strain components, A is the cross-sectional area of the shaft and $\overline{\mathbf{Q}}_{ij}$ equivalent off-axis stiffness matrix of a composite ply with respect to the system $osx\varsigma$.

The variation of the dissipated energy of the cross-section can be expressed as:

$$\delta W_s = \int_A \delta \boldsymbol{\varepsilon}_{x,y}^T \overline{\boldsymbol{\eta}}_{ij} \overline{\mathbf{Q}}_{ij} \boldsymbol{\varepsilon}_{x,y} ds d\varsigma, \tag{2}$$

where $\overline{\boldsymbol{\eta}}_{ij}$ is equivalent off-axis damping matrix of a composite ply with respect to the system $osx\varsigma$.

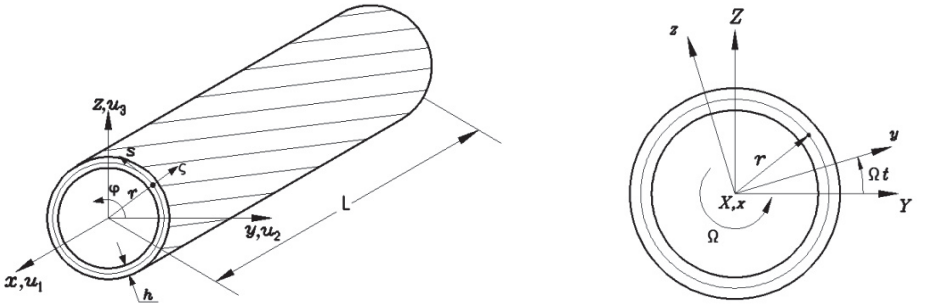

Fig. 1. Geometry and coordinate systems of composite thin-walled shaft

Further, the variation of the kinetic energy of the cross-section with rotating motion is:

$$\delta T_s = \int_A \boldsymbol{\delta}\mathbf{R}^T \mathrm{diag}(\rho)\, \ddot{\mathbf{R}} ds d\varsigma, \tag{3}$$

where $\mathrm{diag}(\rho)$ is a diagonal matrix with components equal to the mass density ρ of a ply.

The position, velocity and acceleration vectors for the deformed shaft are described as:

$$\begin{aligned} \mathbf{R} &= (y+u_2)\mathbf{i} + (z+u_3)\mathbf{j} + (x+u_1)\mathbf{k}, \\ \dot{\mathbf{R}} &= [\dot{u}_2 - \Omega(z+u_3)]\mathbf{i} + [\dot{u}_3 + \Omega(y+u_2)]\mathbf{j} + \dot{u}_1\mathbf{k}, \\ \ddot{\mathbf{R}} &= [\ddot{u}_2 - 2\Omega\dot{u}_3 - \Omega^2(y+u_2)]\mathbf{i} + [\ddot{u}_3 + 2\Omega\dot{u}_2 - \Omega^2(z+u_3)]\mathbf{j} + \ddot{u}_1\mathbf{k}, \end{aligned} \tag{4}$$

where u_1, u_2 and u_3 are the displacements of any point on the the cross-section of the shaft in the x, y and z directions, dot indicates the time derivative of the variable.

2.1. Equivalent cross-section stiffness matrix

To derive the strain energy and dissipated energy of the cross-section, the composite thin-walled beam theory proposed by Berdichevsky et al. [14] is employed in the following.

For the case of no internal pressure acting on the shaft, Eq. (1) can be simplified by using free hoop stress resultant assumption as:

$$\delta U_s = \frac{1}{2}\oint \{\delta\gamma_{11} \quad \delta\gamma_{12}\} \begin{bmatrix} A & B \\ B & C \end{bmatrix} \begin{Bmatrix} \gamma_{11} \\ \gamma_{12} \end{Bmatrix} ds, \tag{5}$$

where $\oint(\cdot)$ denotes the integral around the loop of the mid-line cross-section, and the reduced axial, coupling and shear stiffness A, B and C can be written as:

$$\begin{aligned} &A(s) = A_{11} - \frac{A_{12}^2}{A_{22}}, \quad B(s) = 2\left[A_{16} - \frac{A_{12}A_{26}}{A_{22}}\right], \\ &C(s) = 4\left[A_{66} - \frac{A_{26}^2}{A_{22}}\right], \quad A_{ij} = \sum_{k=1}^{N} \bar{Q}_{ij}^{(k)} (z_k - z_{k-1}), \quad i,j = 1,2,6. \end{aligned} \tag{6}$$

In Eq. (5), δU_s can also be expressed with respect to the u, v, w and φ as:

$$\delta U_S = \delta\Delta^T \mathbf{K}\Delta, \tag{7}$$

where Δ is 4×1 column matrix of kinematic variables defined as $\Delta^T = (u' \quad \varphi' \quad w'' \quad v'')$, and $\mathbf{K}$ is 4×4 symmetric stiffness matrix. Its components k_{ij} are given in Ref. [14].

2.2. Equivalent cross-section damping matrix

Similar to the derivation of the previous cross-section stiffness formulations, the variation of the dissipated energy of the cross-section [15]:

$$\delta W_s = \frac{1}{2}\oint \{\delta\gamma_{11} \quad \delta\gamma_{12}\} \begin{bmatrix} A_d & B_d \\ B_d & C_d \end{bmatrix} \begin{Bmatrix} \gamma_{11} \\ \gamma_{12} \end{Bmatrix} ds, \tag{8}$$

where:

$$\begin{aligned}
A_d &= A_{d11} + \left(\frac{A_{12}^2}{A_{22}^2}\right) A_{d22} - \left(\frac{A_{12}}{A_{22}}\right)(A_{d12} + A_{d21}), \\
B_d &= A_{d16} + A_{d61} + 2\left(\frac{A_{12}A_{26}}{A_{22}^2}\right) A_{d22} - \left(\frac{A_{26}}{A_{22}}\right)(A_{d12} + A_{d21}) - \left(\frac{A_{12}}{A_{22}}\right)(A_{d26} + A_{d62}), \\
\mathrm{C}_d &= 4\left[A_{d66} + \left(\frac{A_{26}^2}{A_{22}^2}\right) A_{d22} - \left(\frac{A_{26}}{A_{22}}\right)(A_{d26} + A_{d62}) \right], \\
A_{dij} &= \int_{-h/2}^{h/2} \bar{\psi}_{il}\bar{Q}_{lj}\, d\varsigma = 2\sum_{k=1}^{N/2} \bar{\psi}_{il}^k\, \bar{Q}_{ij}^k (h_k - h_{k-1}), \quad i,j,l = 1,2,6.
\end{aligned} \tag{9}$$

The variation of the dissipated energy also be expressed in terms of the kinematic variables as:

$$\delta W_s = \delta\Delta^T \mathbf{C}\,\Delta, \tag{10}$$

where $\mathbf{C}$ is 4×4 symmetric damping matrix.

The formulation of its components c_{ij} is analogous to stiffness components k_{ij}, but the terms A, B and C in Eq. (6) should be replaced by the terms A_d, B_d and C_d in Eq. (9), respectively.

2.3. Equivalent cross-section damping matrix

Based on the displacement expressions presented in Ref. [14] and in view of Eqs. (3) and (4), the variation of the kinetic energy of the cross-section can be obtained as:

$$\delta T_s = -(I_1\delta u + I_2\delta v + I_3\delta w + I_4\delta\varphi), \tag{11}$$

where:

$$\begin{aligned}
&I_1 = b_1\ddot{u}, \quad I_2 = b_1(\ddot{v} - 2\Omega\dot{w} - \Omega^2 v) - b_2(2\Omega\dot{\varphi} + \Omega^2) - b_3(\ddot{\varphi} - \Omega^2\varphi), \\
&I_3 = b_1(\ddot{w} + 2\Omega\dot{v} - \Omega^2 w) + b_2(\ddot{\varphi} - \Omega^2\varphi) - b_3(2\Omega\dot{\varphi} + \Omega^2), \\
&I_4 = b_2(\ddot{w} + 2\Omega\dot{v} - \Omega^2 w) - b_3(\ddot{v} - 2\Omega\dot{w} - \Omega^2 v) + (b_4 + b_5)(\ddot{\varphi} - \Omega^2\varphi), \\
&b_1 = \int_A \rho ds d\varsigma, \quad b_2 = \int_A \rho y ds d\varsigma, \quad b_3 = \int_A \rho z ds d\varsigma, \\
&b_4 = \int_A \rho y^2 ds d\varsigma, \quad b_5 = \int_A \rho z^2 ds d\varsigma.
\end{aligned} \tag{12}$$

3. Rigid disks

3.1. Kinetic energy of rigid disks

According to Eqs. (11) and (12) the expression of variation of the kinetic energy of the rigid disks fixed to the shaft is written as:

$$\delta T_D = \sum_{l=1}^{N_D} (I_{1l}^D \delta u + I_{2l}^D \delta v + I_{3l}^D \delta w + I_{4l}^D \delta\varphi)\Delta(x - x_{Dl}), \tag{13}$$

in which:

$$\begin{aligned}
&I_{1l}^D = b_{1l}^D \ddot{u}, \quad I_{2l}^D = b_{1l}^D(\ddot{v} - 2\Omega\dot{w} - \Omega^2 v) - b_{2l}^D(2\Omega\dot{\varphi} + \Omega^2) - b_{3l}^D(\ddot{\varphi} - \Omega^2\varphi),\\
&I_{3l}^D = b_{1l}^D(\ddot{w} + 2\Omega\dot{v} - \Omega^2 w) + b_{2l}^D(\ddot{\varphi} - \Omega^2\varphi) - b_{3l}^D(2\Omega\dot{\varphi} + \Omega^2),\\
&I_{4l}^D = b_{2l}^D(\ddot{w} + 2\Omega\dot{v} - \Omega^2 w) - b_{3l}^D(\ddot{v} - 2\Omega\dot{w} - \Omega^2 v) + (b_{4l}^D + b_{5l}^D)(\ddot{\varphi} - \Omega^2\varphi),\\
&b_{1l}^D = \int_A \rho_l^D \, dsd\varsigma, \quad b_{2l}^D = \int_A \rho_l^D y \, dsd\varsigma, \quad b_{3l}^D = \int_A \rho_l^D \, zdsd\varsigma,\\
&b_{4l}^D = \int_A \rho_l^D \, y^2 dsd\varsigma, \quad b_{5l}^D = \int_A \rho_l^D \, z^2 dsd\varsigma,
\end{aligned} \tag{14}$$

where, ρ_l^D denotes the mass density of the disk l. The symbol $\Delta(x - x_{Dl})$ denotes Dirac delta function, N_D the number of the disks mounted on the shaft and x_{Dl} the location of the lth disk.

3.2. Work of external forces

The external forces include the centrifugal force resulting from the unbalanced rigid disks. The virtual work done by the centrifugal force of rigid disks can be given by:

$$\delta W_e = p_x^u \delta u + p_v^u \delta v + p_z^u \delta w + G_x^u \delta\varphi, \tag{15}$$

where, p_x^u, p_y^u and p_z^u denote centrifugal force per unit length, G_x^u denotes centrifugal moment per unit length. They are given by:

$$\begin{aligned}
&p_x^u = 0, \quad p_y^u = \Omega^2 \cos\Omega t \sum_{l=1}^{N_D} b_{1l}^D \, e_l \Delta(x - x_{Dl}),\\
&p_z^u = \Omega^2 \sin\Omega t \sum_{l=1}^{N_D} b_{1l}^D \, e_l \Delta(x - x_{Dl}), \quad G_x^u = 0,
\end{aligned} \tag{16}$$

where, the mass unbalance associated with disks is assumed as the concentrated masses $b_{1l}^D = \iint_A \rho_l^D dA$ at points with small distances of eccentricity e_l.

4. Equations of motion and approximate solution method

The equations of motion of the composite rotor can be derived by employing the following Hamilton's principle:

$$\int_{t_0}^{t_1} \int_0^L (\delta U_s - \delta T_s - \delta T_D + \delta W_s - \delta W_e) dxdt = 0. \tag{17}$$

In order to find the approximate solution, the quantities $u(x,t)$, $v(x,t)$, $w(x,t)$ and $\varphi(x,t)$ are assumed in the form:

$$\begin{aligned} u(x,t) &= \sum_{j=1}^{N} X_{ju}(t)\alpha_j(x), \quad \varphi(x,t) = \sum_{j=1}^{N} X_{j\varphi}(t)\theta_j(x), \\ v(x,t) &= \sum_{j=1}^{N} X_{jv}(t)\psi_j(x), \quad w(x,t) = \sum_{j=1}^{N} X_{jw}(t)\psi_j(x), \end{aligned} \tag{18}$$

where $\alpha_j(x)$, $\theta_j(x)$ and $\psi_j(x)$ are mode shape functions which fulfill all the boundary conditions of the composite shaft, $X_{ju}(t)$, $X_{j\varphi}(t)$, $X_{jv}(t)$ and $X_{jw}(t)$ are the generalized coordinates.

Substituting Eq. (18) into the governing equations of motion, and applying Galerkin's procedure, the following governing equations in matrix form can be found:

$$\mathbf{M}\ddot{\mathbf{X}} + (\mathbf{C}+\mathbf{G})\dot{\mathbf{X}} + (\mathbf{K}+\mathbf{H})\mathbf{X} = \mathbf{f}, \tag{19}$$

where $X^T = \left(X_{1u}(t), \ldots, X_{Nu}(t), X_{1\varphi}(t), \ldots, X_{N\varphi}(t), X_{1w}(t), \ldots, X_{Nw}(t), X_{1v}(t), \ldots, X_{Nv}(t)\right)$, **M** is the mass matrix, **C** is the damping matrix, **G** is the gyroscopic matrix, **K** the stiffness matrix. **H** is the rotating softening matrix, **f** is the generalized force vector. Their detailed expressions are follows:

$$\mathbf{M} = \begin{bmatrix} -b_1 H_{ij} & 0 & 0 & 0 \\ 0 & -(b_4+b_5)L_{ij} & -b_2 M_{ij} & b_3 M_{ij} \\ 0 & b_2 Q_{ij} & b_1 R_{ij} + b_5 S_{ij} + \sum_{i=1}^{N_D} b_{1l}^D R_{ij}^{Dl} + \sum_{i=1}^{N_D} b_{5l}^D S_{ij}^{Di} & 0 \\ 0 & -b_3 Q_{ij} & 0 & b_1 R_{ij} + b_4 S_{ij} + \sum_{i=1}^{N_D} b_{1l}^D R_{ij}^{Dl} + \sum_{i=1}^{N_D} b_{4l}^D S_{ij}^{Dl} \end{bmatrix}, \tag{20}$$

$$\mathbf{C} = \begin{bmatrix} c_{11}E_{ij} & c_{12}F_{ij} & c_{13}G_{ij} & c_{14}G_{ij} \\ c_{12}I_{ij} & c_{22}J_{ij} & c_{23}K_{ij} & c_{24}K_{ij} \\ c_{13}N_{ij} & c_{23}O_{ij} & c_{33}P_{ij} & c_{34}P_{ij} \\ c_{14}N_{ij} & c_{24}O_{ij} & c_{34}P_{ij} & c_{44}P_{ij} \end{bmatrix}, \tag{21}$$

$$\mathbf{G} = \begin{bmatrix} 0 & 0 & 0 & 0 \\ 0 & 0 & 0 & 0 \\ 0 & 0 & 0 & 2\Omega b_1 R_{ij} + 2\Omega \sum_{i=1}^{N_D} b_{1l}^D R_{ij}^{Dl} \\ 0 & 0 & -2\Omega b_1 R_{ij} - 2\Omega \sum_{i=1}^{N_D} b_{1l}^D R_{ij}^{Dl} & 0 \end{bmatrix}, \tag{22}$$

$$\mathbf{K} = \begin{bmatrix} k_{11}E_{ij} & k_{12}F_{ij} & k_{13}G_{ij} & k_{14}G_{ij} \\ k_{12}I_{ij} & k_{22}J_{ij} & k_{23}K_{ij} & k_{24}K_{ij} \\ k_{13}N_{ij} & k_{23}O_{ij} & k_{33}P_{ij} & k_{34}P_{ij} \\ k_{14}N_{ij} & k_{24}O_{ij} & k_{34}P_{ij} & k_{44}P_{ij} \end{bmatrix}, \tag{23}$$

$$\mathbf{H}=\begin{bmatrix} 0 & 0 & 0 & 0 \\ 0 & (b_4+b_5)L_{ij}\Omega^2 & 0 & 0 \\ 0 & 0 & -b_1R_{ij}\Omega^2-\Omega^2\sum_{l=1}^{N_D}b_{1l}^{D}R_{ij}^{Dl} & 0 \\ 0 & 0 & 0 & -b_1R_{ij}\Omega^2-\Omega^2\sum_{l=1}^{N_D}b_{1l}^{D}R_{ij}^{Dl} \end{bmatrix}, \tag{24}$$

$$\mathbf{f}^{\mathrm{T}}=\left(0,\cdots,0,0,\cdots,0,\Omega^2\sum_{l=1}^{N_D}b_{1l}^{D}e_lB_1^{Dl}\sin\Omega t,\cdots,\Omega^2\sum_{l=1}^{N_D}b_{1l}^{D}e_lB_N^{Dl}\sin\Omega t,\Omega^2\sum_{l=1}^{N_D}b_{1l}^{D}e_lB_1^{Dl}\cos\Omega t,\cdots,\Omega^2\sum_{l=1}^{N_D}b_{1l}^{D}e_lB_N^{Dl}\cos\Omega t\right), \tag{25}$$

where:

$$\begin{aligned} &E_{ij}=\int_0^L\alpha_i\alpha_j''dx,\quad F_{ij}=\int_0^L\alpha_i\theta_j''dx,\quad G_{ij}=\int_0^L\alpha_i\psi_j'''dx,\quad H_{ij}=\int_0^L\alpha_i\alpha_jdx,\\ &I_{ij}=\int_0^L\theta_i\alpha_j''dx,\quad J_{ij}=\int_0^L\theta_i\theta_j''dx,\quad K_{ij}=\int_0^L\theta_i\psi_j'''dx,\quad L_{ij}=\int_0^L\theta_i\theta_jdx,\\ &M_{ij}=\int_0^L\theta_i\psi_jdx,\quad N_{ij}=\int_0^L\psi_i\alpha_j'''dx,\quad O_{ij}=\int_0^L\psi_i\theta_j'''dx,\quad P_{ij}=\int_0^L\psi_i\psi_j''''dx,\\ &Q_{ij}=\int_0^L\psi_i\theta_jdx,\quad R_{ij}=\int_0^L\psi_i\psi_jdx,\quad S_{ij}=\int_0^L\psi_i\psi_j''dx,\quad R_{ij}^{Dl}=\int_0^L\psi_i\psi_j\Delta(x-x_{Dl})dx,\\ &S_{ij}^{Dl}=\int_0^L\psi_i\psi_j''\Delta(x-x_{Dl})dx,\quad B_i^{Dl}=\int_0^L\psi_i\Delta(x-x_{Dl})dx,\quad i,j=1,\ldots,N. \end{aligned} \tag{26}$$

The solution for free vibration of Eq. (19) can be written in the form $\{X\}=\{X_0\}e^{\lambda t}$, from Eq. (19), one can obtain the following characteristic equation:

$$\det(-\lambda^2\mathbf{M}+i\lambda(\mathbf{G}+\mathbf{C})+\mathbf{K}+\mathbf{H})=0. \tag{27}$$

Complex eigenvalue λ can be expressed in the form:

$$\lambda=\sigma+i\omega. \tag{28}$$

The damping natural frequency or whirl frequency of the system is the imaginary part ω, whereas its real part σ gives the decay or growth of the amplitude of vibration. A negative value of σ indicates a stable motion, whereas a positive value indicates an unstable motion, growing exponentially in time.

It should be pointed out that the govering Eq. (19) is derived based on the rotating frame $Oxyz$. In addition, for a CUS (Circumferentially Uniform Stiffness) configuration [16], Eq. (19) involving in terms of displacements can be split into two independent equation systems associated with both flapping bending-sweeping bending and extension-twist motions. The latter is important to helicopter blades. However, we will focus on the flapping bending-sweeping bending coupling only and give all numerical examples with reference to the inertial frame $OXYZ$ in this paper, the resulting govering equation are not shown for the sake of simplicity.

5. Numerical results

5.1. Model verifications

In order to examine the influence of the number of mode shape functions used in the solution

of the equation on the accuracy of the results, the numerical calculations are performed by considering the shaft made of graphite-epoxy whose elastic characteristics are listed in Table 1. The shaft has rectangular cross-section of fixed width $a = 0.32$ m, wall thickness $h = 0.01016$ m and length $L = 4.5952$ m, whose layup is $[\theta]_{16}$ with clamped-free boundary conditions.

Table 1. Mechanical properties of composite material [13]

ρ (kg/m^3)	E_{11} (GPa)	E_{22} (GPa)	G_{12} (GPa)	υ_{12}	η_{l1} (%)	η_{l2} (%)	η_{l6} (%)
1672	25.8	8.7	3.5	0.34	0.65	2.34	2.89

The numerical results of natural frequencies and modal dampings are shown in Tables 2 and 3 for an increasing number of mode shape functions. From these tables, it can be seen that to obtain the accurate results of the first two natural frequencies and dampings of flapping, sweeping and torsional mode no more than five mode shape functions are required. This indicates clearly that the convergence of the present model is quite good.

A comparison of predictions using the present model with those obtained in Ref. [13] are also shown in Table 2 and Table 3. A perfect agreement of numerical results with those in Ref. [13] can be seen.

Table 2. Modal frequencies and damping of cantilever composite box beam: $L/a = 14.36$, $a/b = 5$, $[90]_{16}$

Mode	Natural frequency (Hz)				Damping (%)			
	Present			Ref. [13]	Present			Ref. [13]
	$N = 1$	$N = 3$	$N = 5$		$N = 1$	$N = 3$	$N = 5$	
First flapping	1.80	1.81	1.81	1.80	2.39	2.38	2.38	2.35
Second flapping	–	11.36	11.36	11.5	–	2.37	2.37	2.35
First sweeping	5.67	6.20	6.20	6.50	3.03	2.53	2.53	2.35
Second sweeping	–	39.21	39.21	39.7	–	2.36	2.36	2.37
First torsional	37.83	37.84	37.84	37.7	2.89	2.89	2.89	2.89
Second torsional	112.90	113.01	113.01	113.3	2.82	2.92	2.92	2.89

Table 3. Modal frequencies and damping of cantilever composite box beam: $L/a = 14.36$, $a/b = 5$, $[0]_{16}$

Mode	Natural frequency (Hz)				Damping (%)			
	Present			Ref. [13]	Present			Ref. [13]
	$N = 1$	$N = 3$	$N = 5$		$N = 1$	$N = 3$	$N = 5$	
First flapping	3.12	3.13	3.13	3.10	0.64	0.65	0.65	0.65
Second flapping	–	19.02	19.02	19.8	–	0.69	0.69	0.67
First sweeping	10.80	10.81	10.81	11.0	0.68	0.68	0.68	0.68
Second sweeping	–	68.38	68.38	65.6	–	0.85	0.85	0.90
First torsional	37.83	37.84	37.84	37.7	2.89	2.89	2.89	2.89
Second torsional	112.91	113.01	113.01	113.3	2.33	2.92	2.92	2.89

Table 4. Comparison of the non-dimensional natural frequencies of a rotating cantilever composite shaft

Ω^*	ω_1^*	ω_2^*	ω_3^*	ω_4^*	ω_5^*	ω_6^*
0	3.5160	3.5160	22.0345	22.0345	61.6973	61.6973
Ref. [17]	3.5160	3.5160	22.0340	22.0340	61.6970	61.6970
2	1.5160	5.5160	20.0345	24.0345	59.6973	69.6973
Ref. [17]	1.5160	5.5160	20.0340	24.0340	59.6970	63.6970
3.5	0.0160	7.0160	18.5345	25.5345	58.1973	65.1973
Ref. [17]	0.0000	7.0160	18.5340	25.5340	58.1970	65.1970
4	–	7.5160	18.0345	26.0345	57.6973	65.6973
Ref. [17]	–	7.5160	18.0340	26.0340	57.6970	65.6970
8	–	11.5160	14.0345	3.30345	53.6973	69.6973
Ref. [17]	–	11.5160	14.0340	30.0340	53.6970	69.6970

The non-dimensional natural frequencies of a rotating cantilever composite shaft obtained

using the present model together with those obtained in Ref. [17] are shown in Table 4 for different non-dimensional rotating speeds. A perfect agreement of numerical results with those in Ref. [17] can be seen.

5.2. Results and discussion

In the following numerical example, the composite rotor system is a composite shaft with one rigid disk supported by two rigid bearings at the ends, the disk is at the mid-point of the shaft. The material properties of the composite shaft are those in Table 1. The stacking sequence is $[\pm\theta]_5$. The length, the radius and the wall thickness of the shaft are assumed to be $L = 2.47$ m, $r = 0.0135$ m and $h = 0.001321$ m, respectively whereas those of a uniform rigid disk are $b_{1l}^D = 2.4364$ kg, $e = 5\times10^{-5}$ m, $b_{4l}^D = b_{5l}^D = 0.1901$ kg/m^2. The rotor system is shown in Fig. 2.

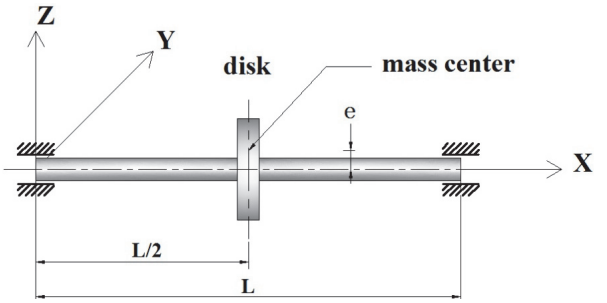

Fig. 2. A composite shaft-rigid disk with rigid bearings

Fig. 3 shows the variation of the first two flexural natural frequencies vs. rotating speed for various ply angles, where, 1F denotes the first forward mode whereas 2F denotes the second forward mode. The synchronous whirl line $\omega = \Omega$ is also presented in the same figure which is the well-known Campbell diagram. The intersection point of the line $\omega = \Omega$ and the flexural natural frequency curves is referred to as the critical speed. The motion corresponding to positive flexural natural frequencies are in forward mode. The backward mode branch of the Campbell diagram with negative value of frequencies is on the lower half $\omega\Omega$-plane and is symmetrical with respect to the Ω axes. The curves corresponding to negative frequencies are not shown in this figure for the sake of simplicity.

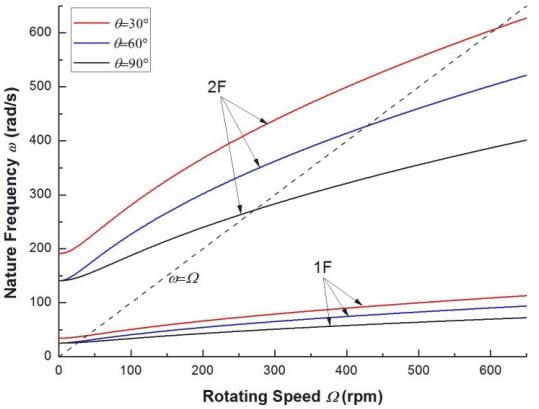

Fig. 3. The Campbell diagram of a composite rotor for various ply angles

From Fig. 3, it is seen that in the inertial frame, natural frequencies of the rotating composite rotor become function of rotating speed as flapping bending and sweeping bending motions are coupled due to the presence of internal damping (there is no the Corilois effect in the inertial

frame). In fact, natural frequencies of a rotating shaft are constant at all rotating speeds in the inertial frame if the influence of internal damping is not considered. The reason is that for the rotating shaft of circular section, the displacement and acceleration vectors and the elastic restoring force always have same direction [18]. As seen in Fig. 3, the effect of the ply angle and rotating speed appear to be more significant for the higher-mode ones.

Fig. 4 shows the variation of the first two flexural dampings vs. rotating speed for various ply angles. It can be seen clearly that as the rotating speed is increased, the dampings of the backward modes decrease and remain negative for all rotating speed, so the backward modes are stable. From the results of Fig. 4, it can be also observed that the dampings corresponding to the forward modes are negative at low rotating speed and increase with increasing rotating speed, and at certain value of rotating speed the dampings vanish and then become positive. Transformation of dampings from negative to positive values marks the onset of unstable motion. The rotating speed corresponding to zero damping is the threshold of instability of the composite rotor. From Fig. 4 it seems that the effect of the ply angle on the damping of the mode 2 is more significant.

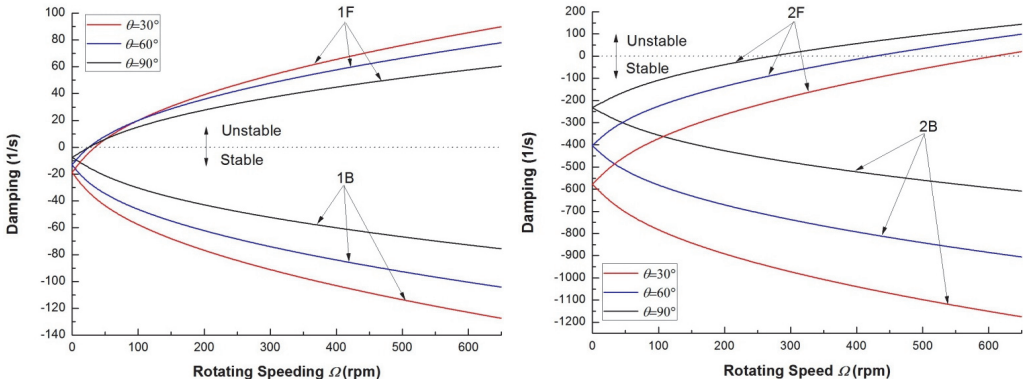

a) Mode 1 b) Mode 2

Fig. 4. The decay plot of a composite rotor for various ply angles

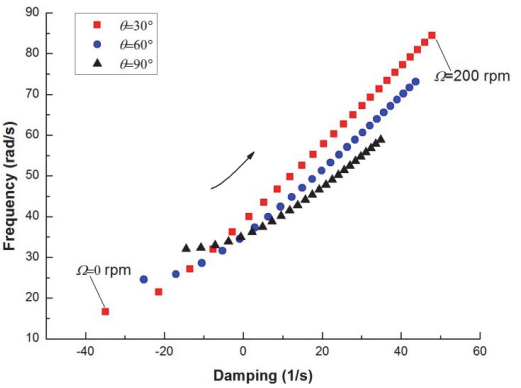

Fig. 5. Root locus of a composite rotor with internal damping

Fig. 5 shows the root locus plot of the complex eigenvalue as a function of rotating speed for various ply angles. For brevity, only the first mode is represented. In the figure the rotating speed is varied from $\Omega = 0.0$ to $\Omega = 200$ rpm in increments of 8.0 rpm. It is readily seen that the curve crosses the imaginary axis into the right hand side of the locus (the unstable region) with the increase of the rotating speed. It is also important to note that in the stable region, the decrease of ply angle will exert a stabilizing effect on the composite rotor, as seen by the curves with lower ply angles being further into the negative region of the locus. In contrast, in the unstable region, the decrease of ply angle promotes further instability, shown by the curves with lower ply angles

being further into the right hand side of the locus.

Fig. 6 shows the effect of ply angle on the first critical rotating speed. It can be seen that as the ply angle increases, the critical rotating speed decreases and the critical speed is maximum at $\theta = 0°$.

Fig. 7 shows the effect of ply angle on the threshold of instability for the flexural mode. It is evident that the general effect of the ply angle on the threshold of instability is similar to that associated with the critical rotating speeds. By comparing Fig. 6 with Fig. 7, it may be noted that for the same ply angle the threshold of instability is larger than the critical rotating speed. This implies that the onset of instability always occurs after the critical rotating speed.

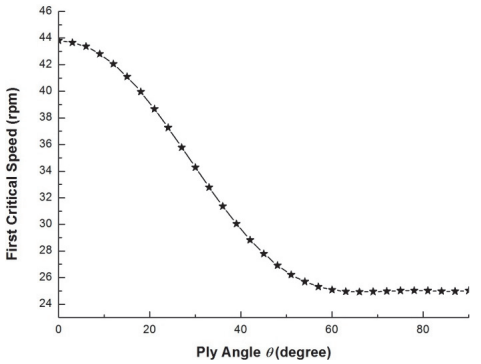

Fig. 6. The variation of the first critical speed with ply angle

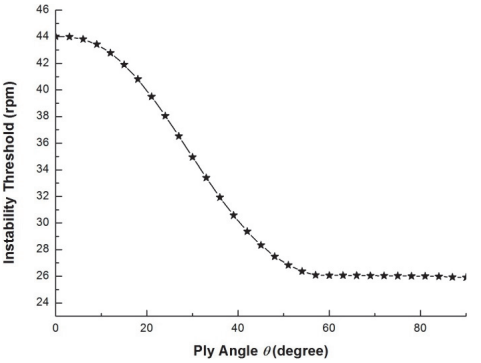

Fig. 7. The variation of thresholds of instability with ply angle

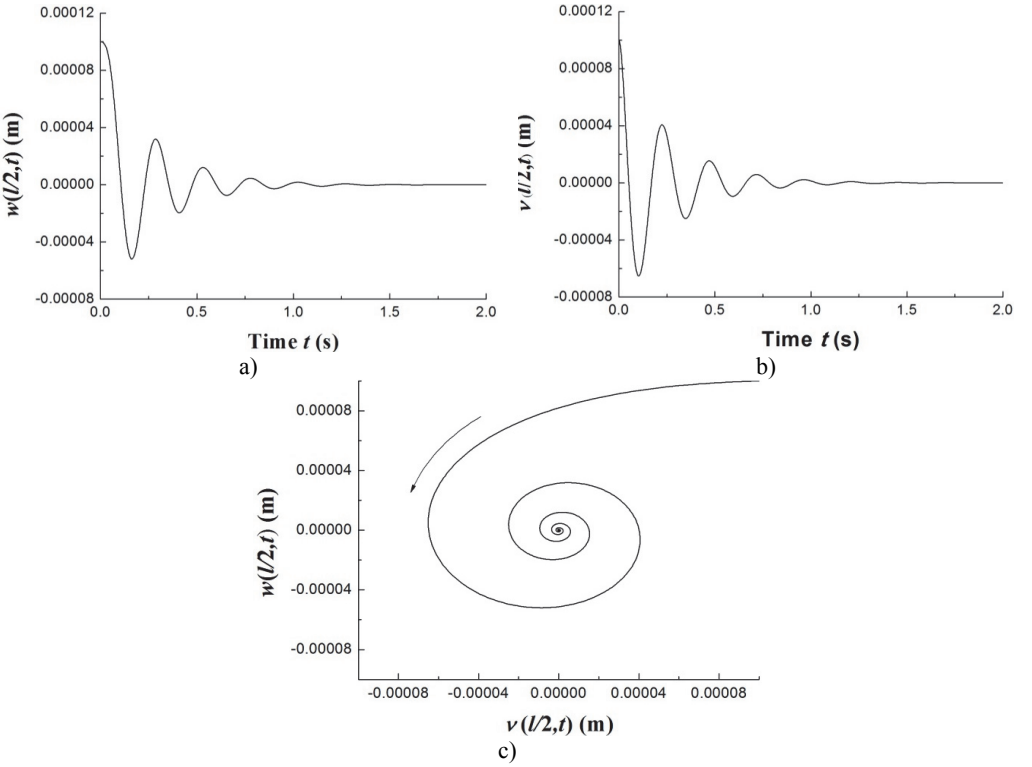

Fig. 8. The time history of deflections and the trajectories of the geometric center of the rigid disk ($\Omega = 20$ rpm)

The transient responses for the geometric center of the rigid disk due to the initial perturbations are calculated by integrating Eq. (20) (with $\{f\} = 0$) using the fourth order Runge-Kutta method. Figs. 8-10 present the time history of deflections and the trajectories of the geometric center of the rigid disk for rotating speeds 20 rpm, 27.89 rpm and 32.5 rpm, respectively. In the simulation, the ply angle $\theta = 45°$, and the initial conditions $X_{jv}(0) = 10^{-5}$, $X_{jw}(0) = 10^{-5}$, $\dot{X}_{jv}(0) = 0$ and $\dot{X}_{jw}(0) = 0$ are specified. Fig. 8 shows that at rotating speed below threshold of instability the oscillation in the two direction can be damped out by internal damping. Fig. 9 shows that when rotating speed is equal to the threshold of instability a whirling response with constant amplitude occurs as internal damping equals to zero in this case. It can also be noted from Fig. 10 that the forward mode of a supercritical composite rotor is unstable since the internal damping becomes positive in this case.

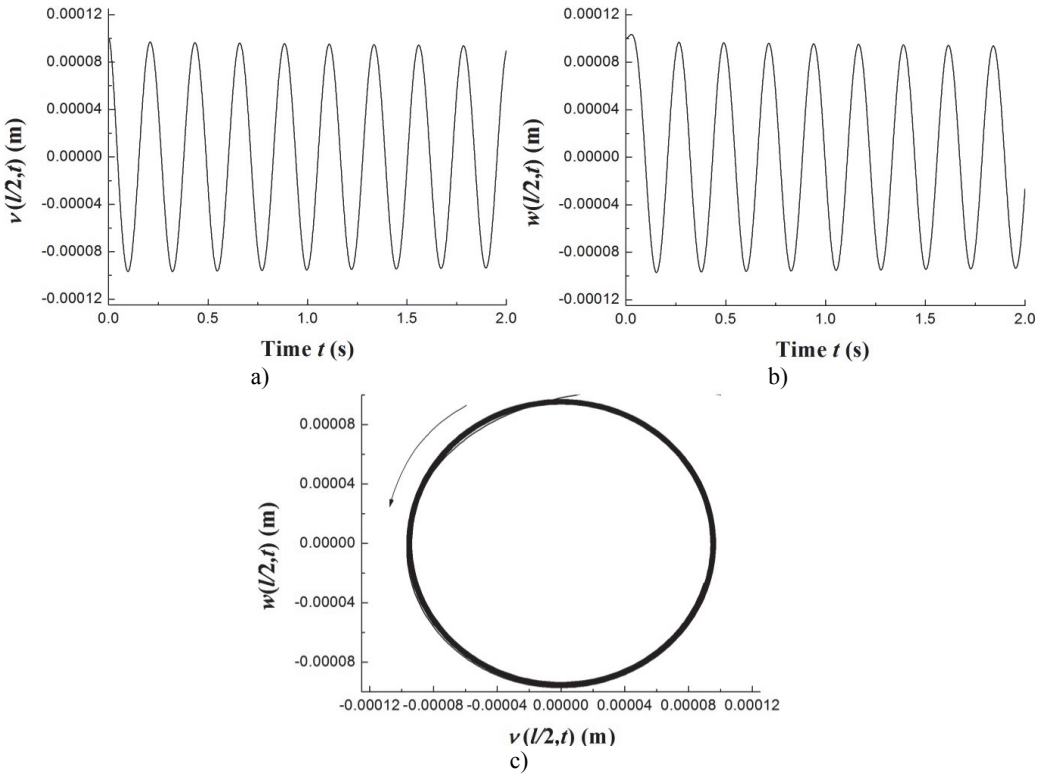

Fig. 9. The time history of deflections and the trajectories of the geometric center of the rigid disk ($\Omega = 27.89$ rpm)

Finally, the steady state response of the composite rotor under the action of unbalance rigid disk is studied. The effect of internal damping on the steady state response is illustrated. In the simulation, the mode superposition method is used to obtain frequency response plots. Fig. 11 shows the two frequency response plots, the plot in dashed line corresponding to the case in which the internal damping are considered and the solid line corresponding to the case in which they are not. As can be seen from Fig. 11, internal damping tends to reduce resonance peak amplitude at critical speeds. This shows that the effect of internal damping on the the forced response is the same as external damping. Fig. 12 shows the effect of ply angle on unbalance steady state response with internal damping. It can be observed that the resonance peak amplitude of the lower mode is much stronger affected by internal damping, on the other hand, the effect of internal damping on the resonance frequency of the higher mode is more significant.

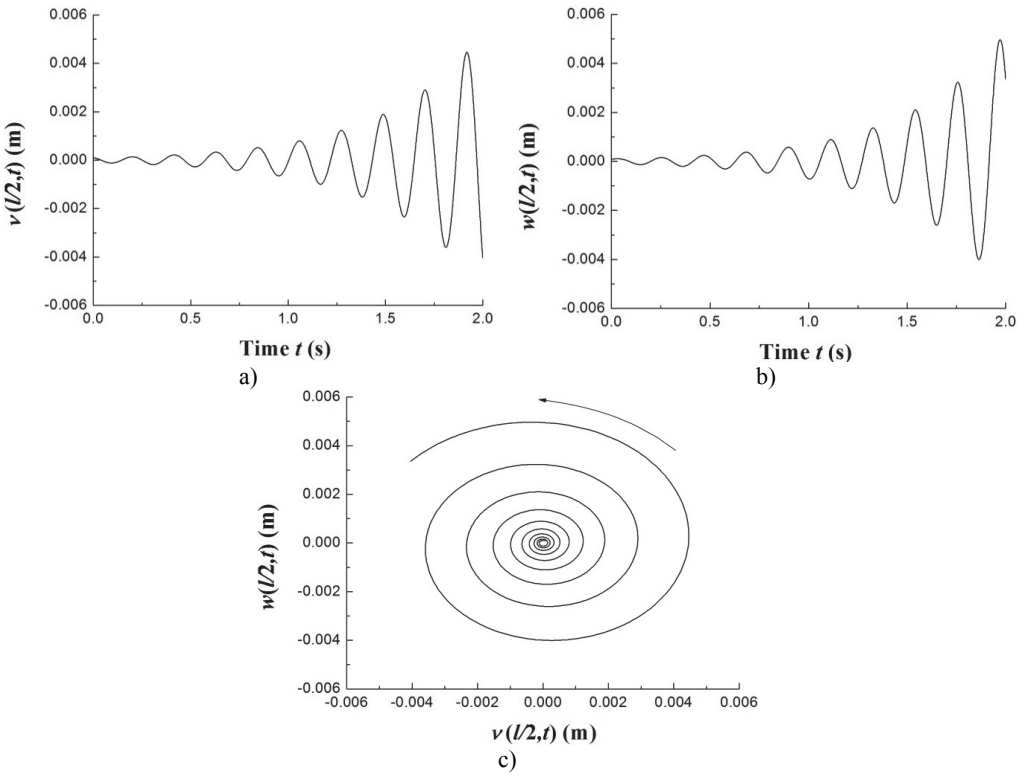

Fig. 10. The time history of deflections and the trajectories of the geometric center of the rigid disk ($\Omega = 32.5$ rpm)

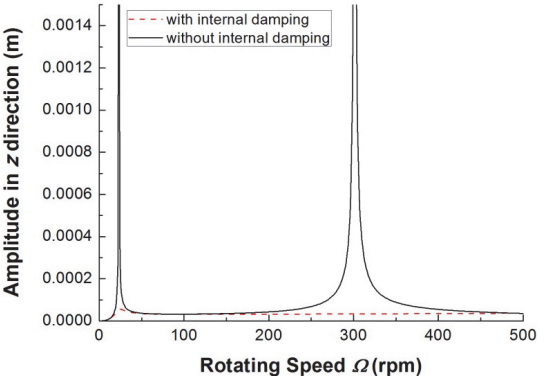

Fig. 11. The frequency response of composite rotor with and without internal damping

6. Conclusions

A model was presented for the study of the dynamical behavior of the composite rotor with internal damping. The presented model was used to predict the natural frequencies, critical rotating speeds, instability thresholds, the transient free vibration responses and the steady state unbalance responses. Theoretical solutions of the free vibration of the system were determined by applying Galerkin's method. From the present analysis and the numerical results, the following main conclusions were drawn:

1) The developed model provides means of predicting of the dynamic behavior of rotating composite rotors with internal damping.

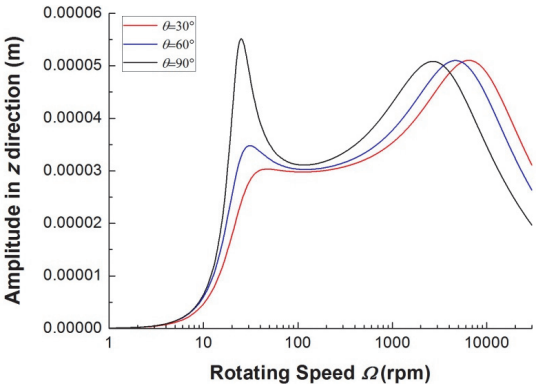

Fig. 12. The frequency response of composite rotor with various internal damping

2) The ply angle affect the steady state unbalance responses and instability behavior of composite rotors significantly.

3) There is an obvious decrease in the first critical rotating speed and instability threshold as the ply angle is increased. And the critical rotating speed and threshold of instability have their maximum values at $\theta = 0°$.

4) The onset of instability always occurs after the critical rotating speed.

Acknowledgements

The research is funded by the National Natural Science Foundation of China (Grant Nos. 11272190), Shandong Provincial Natural Science Foundation of China (Grant Nos. ZR2011EEM031) and Graduate Innovation Project of Shandong University of Science and Technology of China (Grant Nos. YC130210).

References

[1] **Chandra R., Singh S. P., Gupta K.** Damping studies in fiber-reinforced composites-a review. Composite Structures, Vol. 46, Issue 1, 1999, p. 41-51.

[2] **Bucciarelli L. L.** On the instability of rotating shafts due to internal damping. Journal of Applied Mechanics, Vol. 49, 1982, p. 425-434.

[3] **Kimball Jr A. L.** Internal friction theory of shaft whirling. General Electric Review, Vol. 27, 1924, p. 244-251.

[4] **Gunter E. J.** Rotor-bearing stability. Proceedings of the First Turbo-machinery Symposium, 1972, p. 119-141.

[5] **Vance J. M., Lee J.** Stability of high speed rotors with internal friction. ASME Journal of Engineering for Industry, Vol. 96, 1974, p. 960-968.

[6] **Melanson J., Zu J. W.** Free vbration and stability analysis of internally damped rotating shafts with general boundary conditions. ASME Journal of Vibration and Acoustics, Vol. 120, 1998, p. 776-783.

[7] **Montagnier O., Hochard Ch.** Dynamic instability of supercritical driveshafts mounted on dissipative supports-effects of viscous and hysteretic internal damping. Journal of Sound and Vibration, Vol. 305, 2007, p. 378-400.

[8] **Simon A., Flowers G. T.** Adaptive disturbance rejection and stabilization for rotor systems with internal damping. Proceedings of the ASME International Design Engineering Technical Conferences and Computers and Information in Engineering Conference, IDETC/CIE, 2009, San Diego, California, USA.

[9] **Singh S. P., Gupta K.** Composite shaft rotordynamic analysis using a layerwise theory. Journal of Sound and Vibration, Vol. 91, Issue 5, 1996, p. 739-756.

[10] **Kim W., Argento A., Scott R. A.** Forced vibration and dynamic stability of a rotating tapered com posite Timoshenko shaft: bending motions in end-milling operations. Journal of Sound and Vibration, Vol. 246, Issue 4, 2001, p. 563-600.

[11] **Mazzei A. J., Scott R. A.** Effects of internal viscous damping on the stability of a rotating shaft driven through a universal joint. Journal of Sound and Vibration, Vol. 265, Issue 4, 2003, p. 863-885.
[12] **Sino R., Baranger T. N., Chatelet E., Jacque T. G.** Dynamic analysis of a rotating composite shaft. Composites Science and Technology, Vol. 68, 2008, p. 337-345.
[13] **Saravanos D. A., Varelis D., Plagianakos T. S., et al.** A shear beam finite element for the damping analysis of tubular laminated composite beams. Journal of Sound and Vibration, Vol. 291, 2006, p. 802-823.
[14] **Berdichevsky V. L., Armanios E., Badir A. M.** Theory of anisotropic thin-walled closed-cross-section beams. Composites Engineering, Vol. 2, Issue 5-7, 1992, p. 411-432.
[15] **Ren Y. S., et al.** Structure damping of thin-walled composite one-cell beams. Journal of Vibration and Shock, Vol. 31, Issue 3, 2012, p. 141-146,152, (in Chinese).
[16] **Smith E. C., Chopra I.** Formulation and evaluation of an analytical model for composite box-beams. Journal of American Helicopter Society, Vol. 36, Issue 3, 1991, p. 23-25.
[17] **Banerjee J. R., Su H.** Development of a dynamic stiffness matrix for free vibration analysis of spinning beams. Computers and Structures, Vol. 82, 2004, p. 2189-2197.
[18] **Kim J.** Rotation effects on vibration of structures seen from a rotating beam simply supported off the rotation axis. Journal of Vibration and Acoustics, Vol. 128, 2006, p. 328-337.

Yongsheng Ren received the B.S. degree in Engineering Mechanics from Taiyuan University of Technology, China, in 1982 and M.S. degree in General Mechanics from Southeast University, China, in 1989. He received his Ph.D. degree in Solid Mechanics from Nanjing University of Aeronautics and Astronautics, China, in 1992. He is a professor at College of Mechanical and Electronic Engineering, Shandong University of Science and Technology, China. His research interests include nonlinear dynamics, smart materials, vibration and shock control and aeroelasticity, etc.

Xingqi Zhang received the Bachelor's degree in Qindao Binhai College, Qingdao, China, in 2012. Now he is a Master Graduate student with Shandong University of Science and Technology, Qindao, China. His current research interests include system dynamics, vibration control.

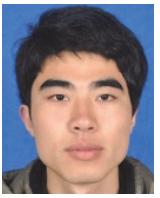

Yanghang Liu received the Bachelor's degree in Qindao Binhai College, Qingdao, China, in 2012. Now he is a Master Graduate student with Shandong University of Science and Technology, Qindao, China. His current research interests include system dynamics, nonlinear vibration.

Xiulong Chen received the B.S. degree in Mechatronic Engineering from Hebei Normal University of Science and Technology, China, in 1999 and M.S. degree in Mechanical Design from Yanshan University, China, in 2002. He received his Ph.D. degree in Mechatronic Engineering from Yanshan University, China, in 2005. He is an associate professor at College of Mechanical and Electronic Engineering, Shandong University of Science and Technology, China. His research interests include nonlinear dynamics, smart materials and parallel mechanism, etc.